

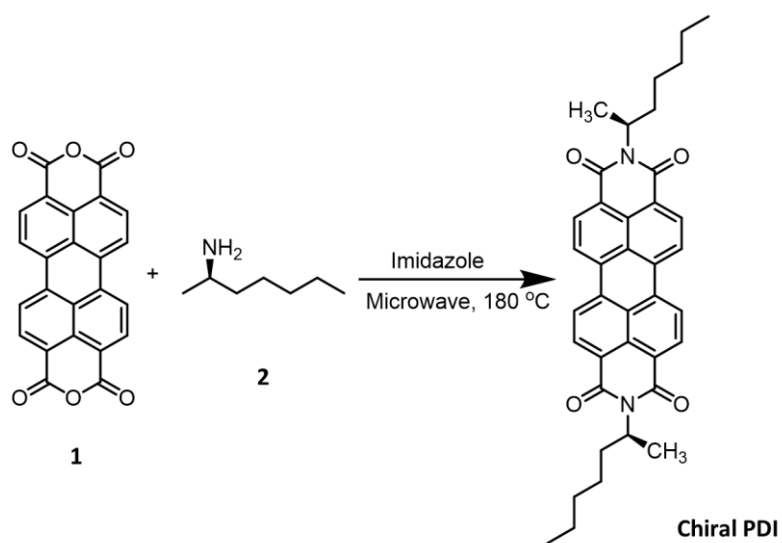
Supplementary Information

Chiral supramolecular polymer functionalized two-dimensional transition metal-based catalyst for enhancing the electrochemical water splitting via spin-polarized charge transfer

Utkarsh, Sai Rachana Pramatha, Anujit Balo, Utpal Kumar Gosh, Venkata Rao Kotagiri,
Koyel Banerjee Ghosh**

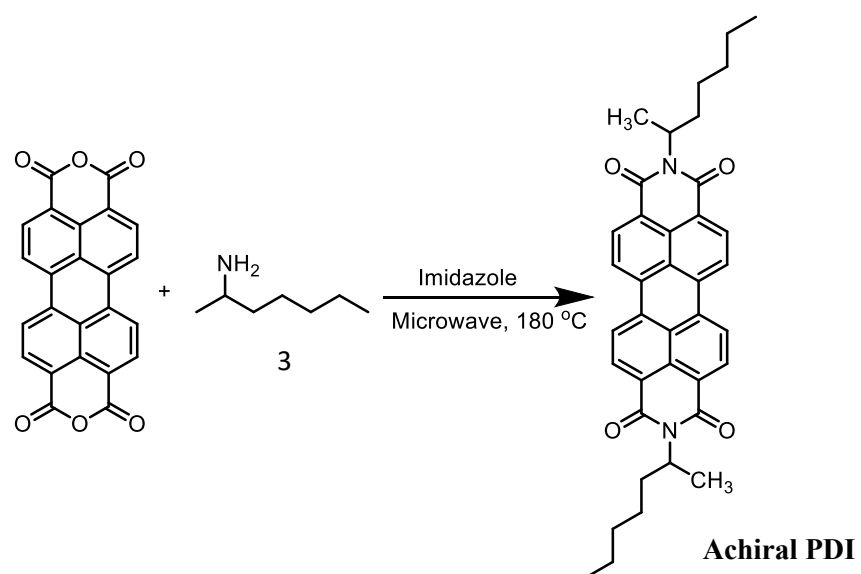
Department of Chemistry, Indian Institute of Technology Hyderabad, Telangana 502284,
India

Synthesis of Chiral-S-PDI

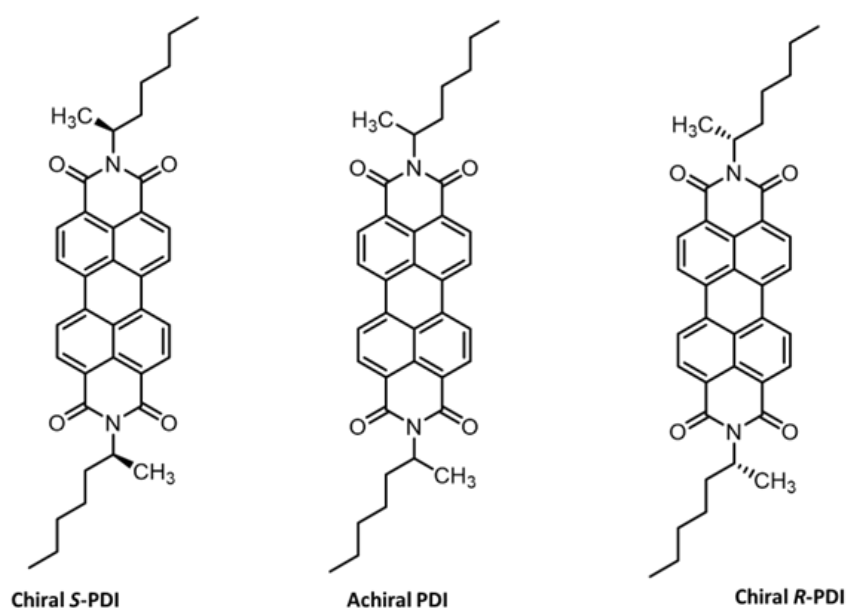


Scheme 1: Synthesis of Chiral S-PDI.

Synthesis of Achiral PDI



Scheme 2: Synthesis of Achiral PDI.



Scheme 3: Structure of chiral *S*-PDI, achiral PDI, and chiral *R*-PDI.

Characterization using NMR

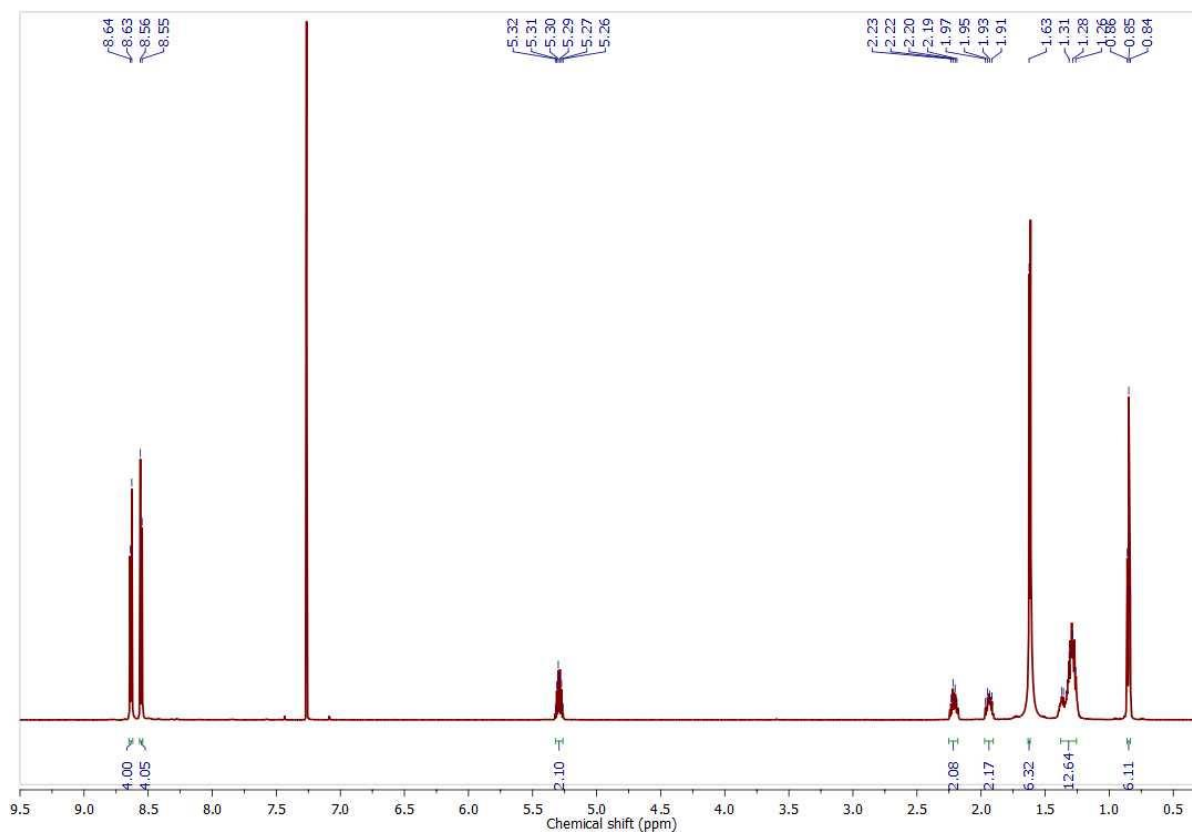


Figure S1. ^1H NMR spectrum of Chiral PDI.

^1H NMR (600 MHz, CDCl_3) δ 8.63 (d, $J = 7.9$ Hz, 4H), 8.55 (d, $J = 8.1$ Hz, 4H), 5.32 – 5.25 (m, 2H), 2.21 (m, $J = 8.6$ Hz, 2H), 1.94 (m, $J = 10.3$ Hz, 2H), 1.63 (d, 6H), 1.39 – 1.24 (m, 12H), 0.85 (t, $J = 7.1$ Hz, 6H).

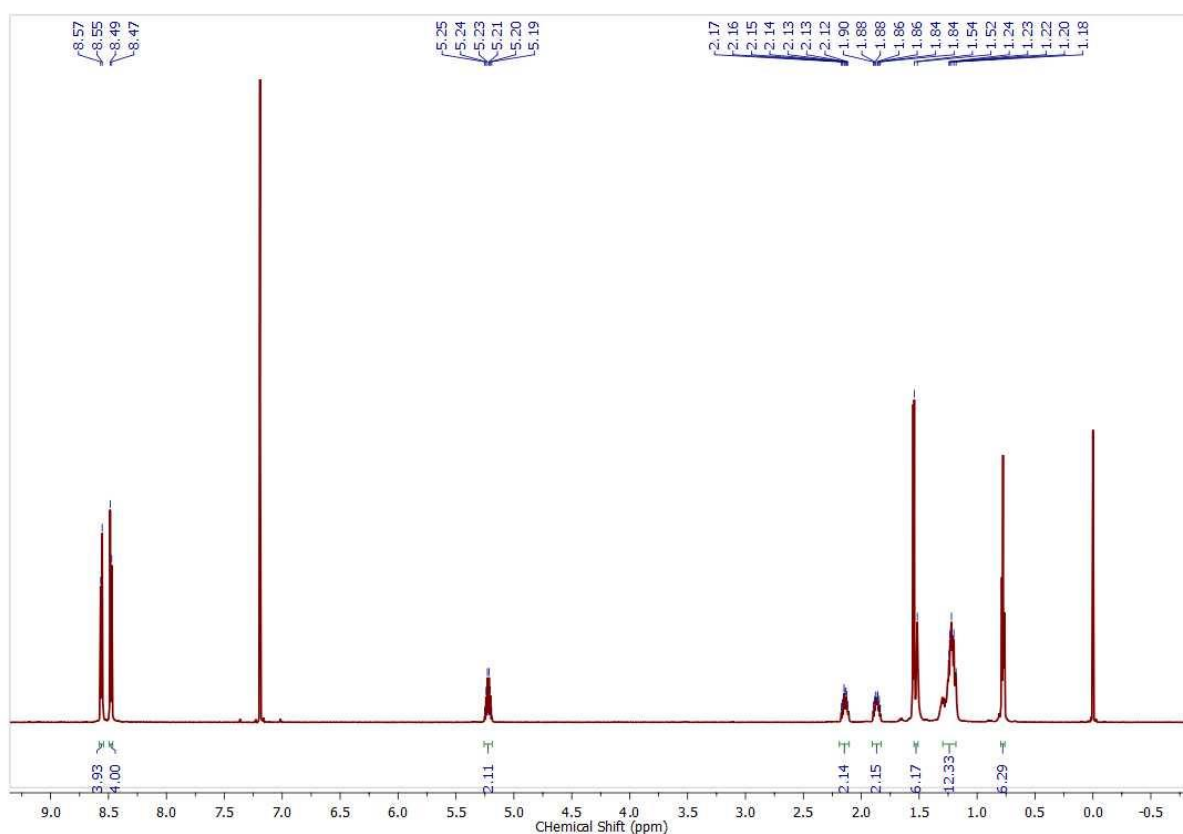


Figure S2. ^1H NMR spectrum of Achiral PDI.

^1H NMR (600 MHz, CDCl_3) δ 8.56 (d, $J = 7.9$ Hz, 4H), 8.48 (d, $J = 8.0$ Hz, 4H), 5.26 – 5.19 (m, 2H), 2.20 – 2.06 (m, 2H), 1.86 (dt, $J = 12.0, 4.4$ Hz, 2H), 1.53 (d, $J = 15.5$ Hz, 6H), 1.34 – 1.16 (m, 12H), 0.78 (t, $J = 7.0$ Hz, 6H).

Formation of Achiral supramolecular PDI-based polymer.

As, the amine employed in the synthesis of achiral PDI is a racemic mixture of *R*-2-heptylamine and *S*-2-heptylamine and 2 equivalent of amine reacts with 1 equivalent of PTCDA, the resulting product should contain a mixture of 25% chiral *S*-PDI, 25% chiral *R*-PDI and 50% achiral *R/S*-PDI (PDI with one side *R*-2-heptylamine and other side *S*-2-heptylamine side chains). This is true for the monomeric solution (Figure S3).

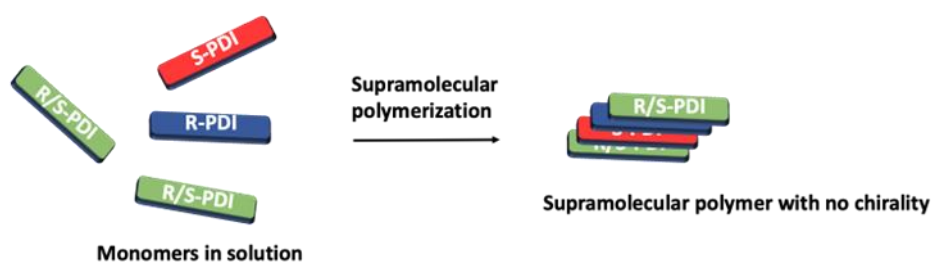


Figure S3: Co-assembly of *S*-PDI, *R*-PDI and *R/S*-PDI leading to the formation of a supramolecular polymer with no chirality.

However, we have to appreciate the fact that during the time of the formation of the supramolecular assembly from this monomeric solution, a variety of possibilities of combination among the monomers may emerge, e.g. *R*-PDI interacting with *R*-PDI, may form an *R*-helix, or *S*-PDI interacting with *S*-PDI, may form a *S*-helix. Moreover, chiral PDIs do not have any preference to interact only among themselves to form chiral supramolecular polymers. For example, *R*-PDI can interact with *S*-PDI or *R/S*-PDI, though this interaction will not lead to the formation of helical structures (Figure 1). Hence, if we observe the probability of the formation of pure *R*-helix from *R*-PDI or *S*-helix from *S*-PDI, it will be effectively reduced to 0.25. Hence, the supramolecular assembly may contain 6.25 % of *R*-helix and 6.25% of *S*-helix.

Electrochemical active surface area (ECSA) determination

The electrochemically active surface area (ECSA) of all the electrodes has been estimated in 1 M KOH solution using the following formula.

$$ECSA = \frac{C_{dl}}{C_s}$$

Where, C_{dl} is the double-layer capacitance and C_s is the specific capacitance.

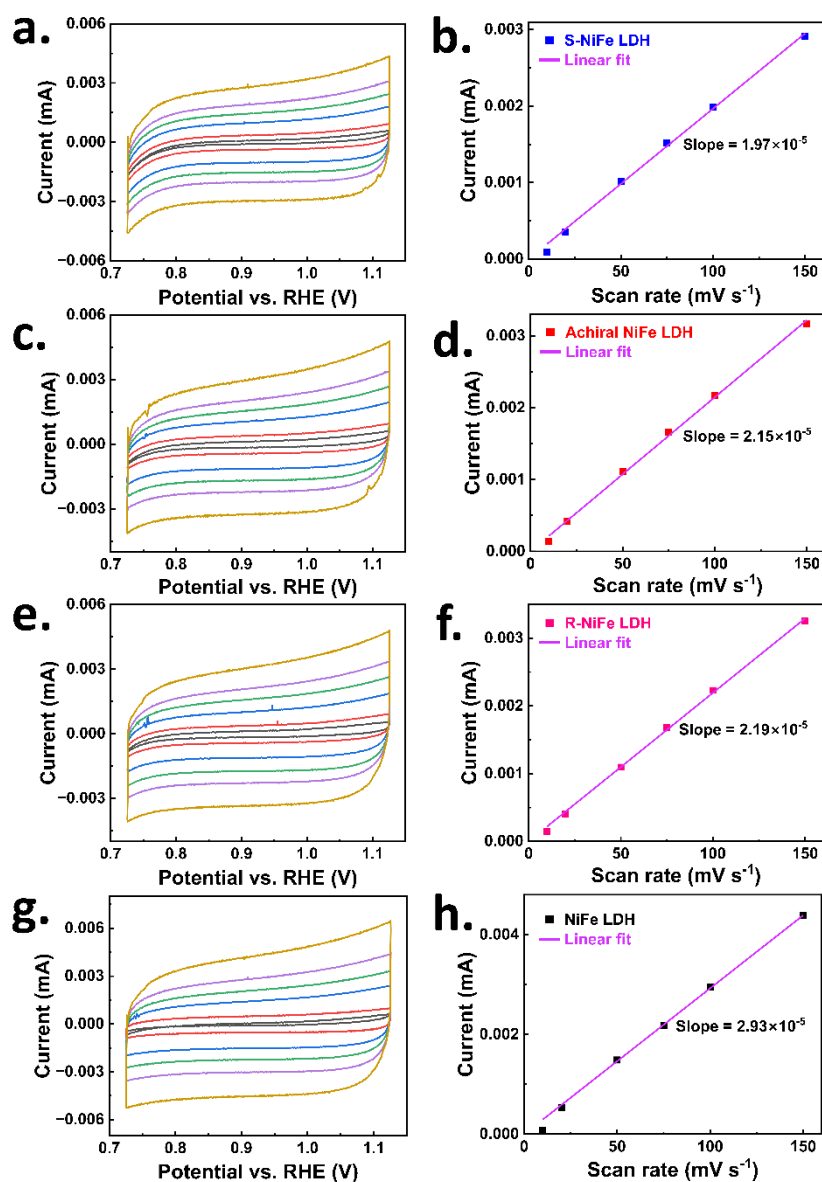


Figure S4. CV plots obtained with scan rates of 10 mV/s (black line), 20 mV/s (red line), 50 mV/s (blue line), 75 mV/s (green line), 100 mV/s (purple line), 150 mV/s (yellow line) and plots of the average current at 0.93 V vs. scan rates of (a, b) S-NiFe LDH (c, d) Achiral NiFe LDH, (e, f) R-NiFe LDH and, (g, h) NiFe LDH coated electrodes.

The double-layer capacitance has been evaluated by carrying out the cyclic voltammetry in the non-Faradaic region. From the slope of the current vs. scan rate, the double-layer capacitance has been evaluated (Figure S3). The specific capacitance which is defined as the capacitance of an atomically smooth planar surface of the material per unit area under identical electrolyte conditions is considered here as $40 \mu\text{F cm}^{-2}$.¹ The ECSA obtained from this method is normalized with respect to geometrical area which was found to be 0.3, 0.27, 0.29 and 0.28 per cm^2 geometrical area respectively for NiFe LDH, S-NiFe LDH, R-NiFe LDH and the achiral NiFe LDH.

Error bars to check the reproducibility of the result

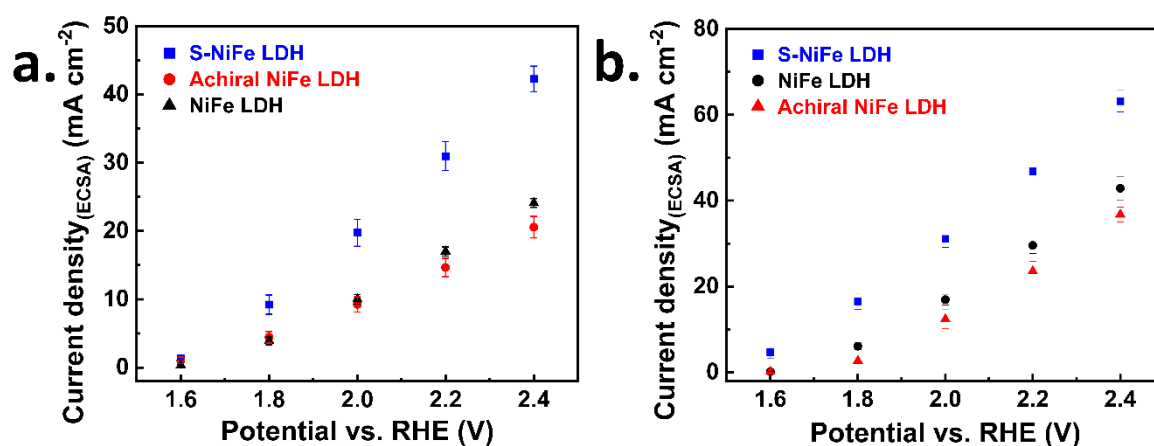


Figure S5. a) Error bar in 0.1 M KOH. b) Error bar in 1 M KOH. Three independent measurements were carried out using all the electrodes.

Control experiment to evaluate the electrocatalytic property of only chiral (*S*), achiral PDI, and catalyst-coated electrode.

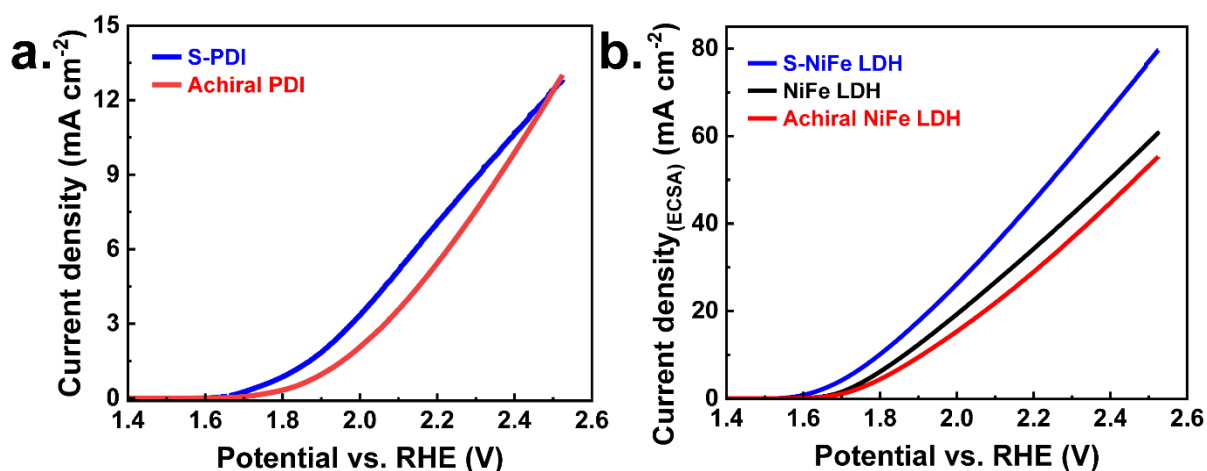


Figure S6. a) Linear sweep voltammograms of chiral *S*-PDI (blue solid line) and achiral PDI (red solid line) coated on FTO carried out in 1 M KOH solution with a scan rate of 50 mV s⁻¹, here geometrical area is considered as an electrochemical active surface area. b) Linear sweep voltammograms of NiFe LDH (black solid line), *S*-NiFe LDH (blue solid line), and achiral NiFe LDH (red solid line) coated on FTO carried out in 1 M KOH solution with a scan rate of 50 mV s⁻¹.

Stability study of the catalysts

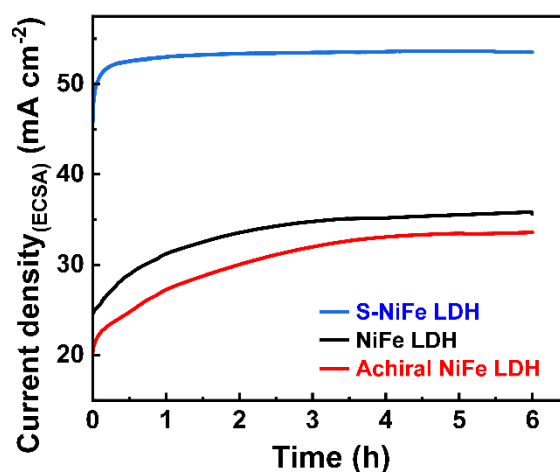


Figure S7. Stability plot, current density vs. time for *S*-NiFe LDH, NiFe LDH, and achiral NiFe LDH integrated electrodes.

Formation of spin-antiparallel intermediates from racemic helices during the electrochemical oxygen generation process

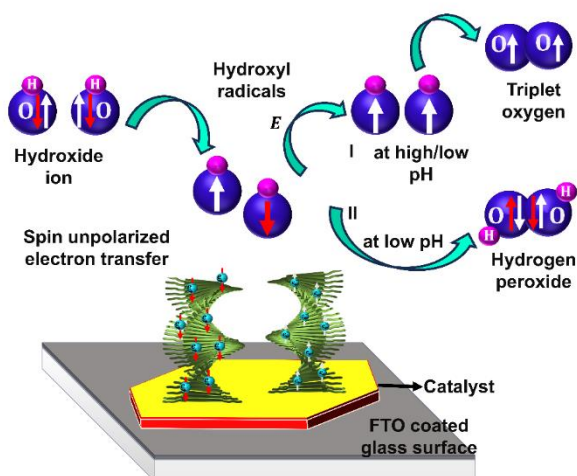


Figure S8: Spin-polarized charge transfer from the racemic mixture of R and S helices and formation of spin-antiparallel intermediate.

Cyclic voltammetry study using $\text{Fe}^{2+/3+}$ redox couple using chiral and achiral electrodes

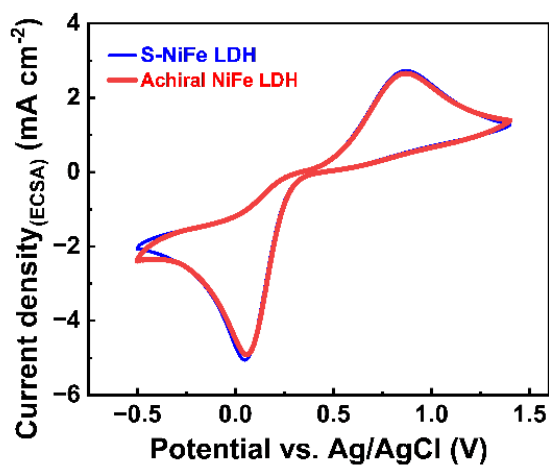


Figure S9: Cyclic voltammograms of S-NiFe LDH and achiral NiFe LDH, $\text{Fe}^{3+/2+}$ redox couple in 0.1 M KCl solution with a scan rate of 50 mV s^{-1} .

Inductive Coupled Plasma measurement

For digestion, we took 50 mg of catalyst in HNO₃ (10 ml) and HCl (1 ml) solution and transferred this solution to a vessel, and heat at 200 °C for 20 min. After cooling it down to room temperature, we diluted it by 3% HNO₃ to 1 ppm. For calibration of the instrument, we used IV-ICP MS 71A (10 ppm 3% HNO₃) standard.

Reference:

[1] C. C. L. McCrory, S. Jung, J. C. Peters and T. F. Jaramillo, *J. Am. Chem. Soc.*, 2013, **135**, 16977–16987.